Dalton Transactions

Bridging Cyanides from Cyanoiron Metalloligands to Redox-active Dinitrosyl Iron Units

Journal:	*Dalton Transactions*
Manuscript ID	DT-ART-05-2018-001761.R1
Article Type:	Paper
Date Submitted by the Author:	04-Jun-2018
Complete List of Authors:	Ghosh, Pokhraj; Texas A&M University College Station, Chemistry Quiroz, Manuel; Texas A&M University College Station, Chemistry Pulukkody, Randara; Texas A&M University College Station, Chemistry Bhuvanesh, Nattamai; Texas A&M University, Department of Chemistry Darensbourg, Marcetta; Texas A&M Univ, Chemistry

Bridging Cyanides from Cyanoiron Metalloligands to Redox-active Dinitrosyl Iron Units

Pokhraj Ghosh[#,‡], Manuel Quiroz[#,‡], Randara Pulukkody[#], Nattamai Bhuvanesh,[#] and Marcetta Y. Darensbourg[#,*]

[#]Department of Chemistry, Texas A & M University, College Station, Texas 77843, United States
[‡]Equally contributing authors

Abstract

Cyanide, as an ambidentate ligand, plays a pivotal role in providing a simple diatomic building-block motif, for controlled metal aggregation, M-CN-M'. Specifically, the inherent hard-soft nature of the cyanide ligand, *i.e*., hard-nitrogen and soft-carbon centers, are electronic handles for binding Lewis acids following the hard-soft acid-base principle. Studies by Holm and Karlin showed structural and electronic requirements for cyanide-bridged (por)Fe^{III}-CN-$Cu^{II/I}$ (por = porphyrin) molecular assemblies as biomimetics for cyanide-inhibited terminal quinol oxidases and cytochrome-C oxidase. The dinitrosyliron unit (DNIU) that exists in two redox states, $\{Fe(NO)_2\}^9$ and $\{Fe(NO)_2\}^{10}$, draws significance as an electronic analogy of Cu^{II} and Cu^{I}, d^9 and d^{10}, respectively. In similar controlled aggregations, L-type [(η^5-C_5R_5)Fe(dppe)(CN)] (dppe = diphenyl phosphinoethane; R = H and Me) have been used as N-donor, μ-cyanoiron metalloligands to stabilize the DNIU in two redox states. Two bimetallic [(η^5-C_5R_5)(dppe)Fe^{II}-CN-$\{Fe(NO)_2\}^9$(sIMes)] complexes, **Fe-1 (**R = H) and **Fe*-1** (R = CH_3), showed dissimilar $Fe^{II}C{\equiv}N$-$\{Fe(NO)_2\}^9$ angular bends due to the electronic donor properties of the [(η^5-C_5R_5)Fe(dppe)(CN)] μ-cyanoiron metalloligand. A trimetallic [(η^5-C_5Me_5)(dppe)Fe^{II}-CN]$_2$-$\{Fe(NO)_2\}^{10}$ complex, **Fe*-2**, engaged two bridging μ-cyanoiron metalloligands to stabilize the $\{Fe(NO)_2\}^{10}$ unit. The lability of the Fe^{II}-CN-$\{Fe(NO)_2\}^{9/10}$ bond was probed by suitable X-type (Na^+SPh^-) and L-type (PMe_3) ligands. Treatment of **Fe-1** and **Fe*-1** with PMe_3 accounted for a reduction-induced substitution at the DNIU, releasing [(η^5-C_5R_5)Fe(dppe)(CN)] and the N-heterocyclic carbene, and generated $(PMe_3)_2Fe(NO)_2$ as the reduced $\{Fe(NO)_2\}^{10}$ product.

Introduction

In a comprehensive, 2007 review (now approaching 1000 citations), Kim Dunbar highlighted complex magnetic phenomenon such as photomagnetism and spin crossover that are displayed in single-molecule magnets based on cyanide as an ambidentate ligand for multimetallic assemblies.[1] Dunbar also noted instances of linkage isomerism by the electronically versatile cyanide ligand, largely applied to extended arrays of metal cyanides.[2,3] Applications of cyanide as ligand in bioinorganic chemistry also abound, typically with single binding sites that use cyanide as a detector of metal-containing enzyme

active sites via inhibition that correlates with spectral evidence. For example, in the course of developing small molecule models of the O_2-inhibited CuFe site of cytochrome-C oxidase, Holm[4-8] as well as Karlin,[9] found CN to bridge an iron-porphyrin to copper, the latter installed with tetra- or tri-nitrogen donor ligation. Dependent on the oxidation state of Cu, different cyanide orientations, (por)Fe^{III}-CN-Cu^{II} and (por)Fe^{III}-NC-Cu^{I} arose from the same (por)Fe^{III}(CN) donor precursors; the preference of C by the softer Cu^{I} receiver overcame the barrier for cyanide flipping or linkage isomerization. In contrast, in a broad series of single cyanide-bridged organo-bimetallic complexes explored by Vahrenkamp, *et al*., no such isomerism was observed; the orientation of the cyanide bridge was determined solely by the precursors, even when the linkage isomer was accessible by the opposite choice of precursors, and found to be stable.[10,11]

Scheme 1. Adduct formation between Fe(III)porphyrin and Cu(I) and Cu(II).[4-9]

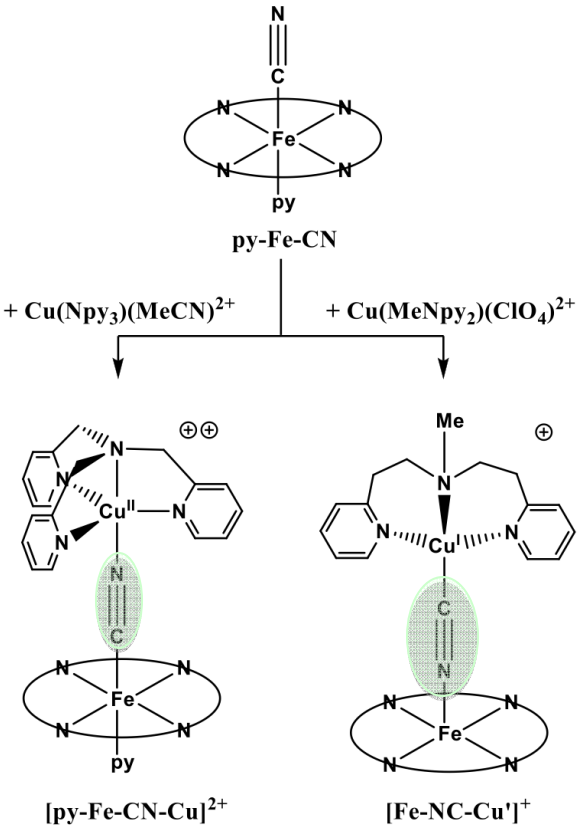

Cyanide linkage isomerism, or flipping, was recently invoked to account for spectral properties of hybrid proteins, i.e., synthetic analogues of the diiron subsite of the H cluster in [FeFe]-hydrogenase that are accepted by an apo-maturase precursor, Hyd-F, on which the native diiron subsite is proposed to be synthesized.[12] Our attempts to mimic such a possibility included a set of cyanide-bridged [FeFe]–CN–Fe complexes as models of the [FeFe]-NC-[4Fe-4S] arrangement in the [FeFe]-HydF.[13] Consistent with the Vahrenkamp report, *vida supra*, the precursors, an Fe-CN donor and an Fe-acceptor with readily accessible open site, determined the orientation of cyanide in the Fe-CN-Fe' bridge.[10,13] Calculations using DFT found that a high kinetic barrier for CN isomerization in [FeFe]–CN–Fe ⇌ [FeFe]–NC–Fe units, rather than thermodynamic ground state differences, accounted for the stability of the once-formed cyanide bridge.[13]

Drawing on the Holm design which gave positive evidence for cyanide flipping,[5] we have recently prepared model diiron carbonyl complex cyanide bridged to copper(I) and copper(II) in nitrogen ligation.[14] Here cyanide flipping was observed as the [FeFe]-CN-Cu adducts were formed, and, as seen in the Holm and Karlin studies, the oxidation state of copper was the determinant of the final arrangement,

i.e., [FeFe]-NC-Cu^{I} or [FeFe]-CN-Cu^{II}.[14] Impressed with the similarity of chemical features and coordination preferences of Cu^{I} and Cu^{II} , d^{10} and d^{9}, respectively, and the dinitrosyliron units (DNIU) in reduced and oxidized forms, $\{Fe(NO)_2\}^{10}$ and $\{Fe(NO)_2\}^{9}$, (Enemark-Feltham notation)[15], we have designed $[Fe^{II}\text{-}(CN)]_n\text{-}\{Fe(NO)_2\}^{9/10}$ bi-/tri-metallics, as a synthetic endeavour for understanding the ambidentate binding modes of cyanide to redox non-innocent units. For example, Cu^{I} and $\{Fe(NO)_2\}^{10}$ are known to be stabilized by soft, L-type donors, while the oxidized Cu^{II} or $\{Fe(NO)_2\}^{9}$ 'prefer' X-type ligands. There are typically easy routes to redox interchanges. This has been observed for the stabilization of $\{Fe(NO)_2\}^{9/10}$ by redox-active metallodithiolates (MN_2S_2) as L-type ligands.[16,17] Herein, neutral, L-type $[(\eta^5\text{-}C_5R_5)Fe(dppe)(CN)]$ (dppe = diphenyl phosphinoethane; R = H[18] and Me) μ-cyanoiron ligands were employed as N-donors to stabilize DNIUs in two redox states $\{Fe(NO)_2\}^{9/10}$, in order to discern the ambidentate binding modes of the bridging cyanide.

Results and Discussion

Synthesis. Scheme 2 displays the synthetic approach to Fe^{II}-CN-$\{Fe(NO)_2\}^{9/10}$ units composed of $(\eta^5\text{-}C_5R_5)Fe(dppe)(CN)$ (where R = H[18] and CH_3; **Fe'-CN** and **Fe*-CN**, respectively) and the $Fe(NO)_2$ unit from well established synthons $\{Fe(NO)_2\}^{9}$ and $\{Fe(NO)_2\}^{10}$.[19,20] On addition of CH_2Cl_2 solvent at 22°C to a mixture of the precursors as solids, the cyanide-bridged bimetallic products, $(dppe)(\eta^5\text{-}C_5R_5)Fe\text{-}CN\text{-}Fe(NO)_2(IMes)]^{+}$ $[BF_4]^{-}$ (where R = H and CH_3; **Fe-1** and **Fe*-1**, respectively), formed immediately in near quantitative yields. The efficiency of this reaction stresses the prominent reactivity / electrophilicity of the

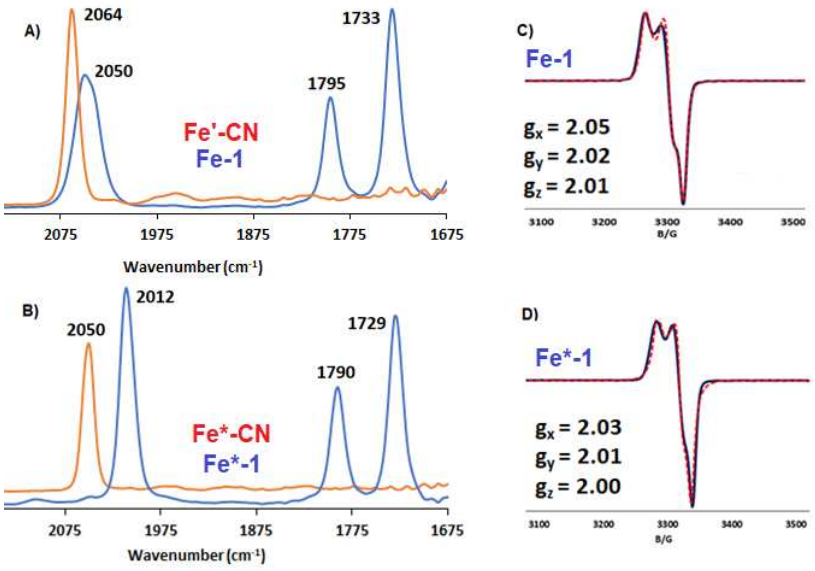

Figure 1. Overlay of IR spectra in diatomic ligand region recorded in CH_2Cl_2 solution of A) $(dppe)(\eta^5\text{-}C_5H_5)Fe(CN)$ (red) and the **Fe-1** (blue) product; B) of $(dppe)(\eta^5\text{-}C_5Me_5)Fe(CN)$ (red) and the **Fe-1*** (blue) product. Frozen CH_2Cl_2 solution EPR spectra of **Fe-1** (C, 5 K) and **Fe-1*** (D, 7 K). The *g* values are from simulations shown in red trace. The coupling constant A (I = 1, for ^{14}N) was found to be 13 and 14 MHz, respectively.

(IMes)Fe(NO)$_3^+$ synthon which has been effective for forming a number of heterobimetallic complexes.[20, 21] The carbene-bound dinitrosyliron unit (DNIU) acts as a receiver for the N-centered cyanide-based organoiron ligand which was isolated in {Fe(NO)$_2$}^{9} redox state.

The cyanide bridged bimetallic complexes were isolated as dark purple crystalline solids. The molecular structures, as obtained from x-ray diffraction, are depicted in Scheme 1 and are described in detail below. The *ν*(CN) stretching frequencies of the bimetallic products, **Fe-1** and **Fe*-1**, at 2050 and 2012 cm^{-1}, respectively, showed a bathochromic shift to lower wavenumbers, by 14 and 38 cm^{-1}, compared to the starting materials, [(dppe)(η^5-C$_5$R$_5$)Fe(CN)], R = H and CH$_3$, respectively, Figure 1. The greater shift in *ν*(CN) stretching frequencies for **Fe*-1** compared to **Fe-1**, is ascribed to the increased electron-donor ability of (dppe)(η^5-C$_5$Me$_5$)Fe(CN) over (dppe)(η^5-C$_5$H$_5$)Fe(CN). The decrease in *ν*(CN) stretching frequencies upon adduct formation, reflects addition of electron density into the empty p_π* orbital on CN, indicating the μ-cyano ligand functions as a π-acid.[5] Along with the *ν*(CN) IR spectral monitor, the *ν*(NO) also indicated the completeness of reaction. Further, the shifts of *ν*(NO) are readily interpreted according to the drain of electron density from the [(dppe)(η^5-C$_5$R$_5$)Fe(CN)] metallo-cyanide as ligand, with concurrent enhancement of electron density at the Fe(NO)$_2$ acceptor. The effect of η^5-C$_5$Me$_5$ over η^5-C$_5$H$_5$ was observed in the lowering of *ν*(NO) stretching frequencies by 5 cm^{-1}, in case of the former, in the bimetallic products.

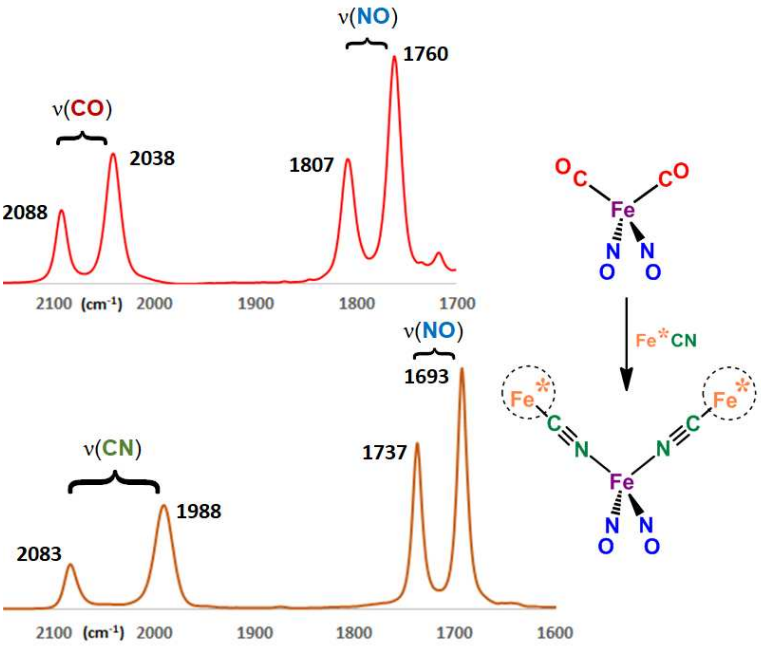

Figure 2. Diatomic ligand region infrared spectra for CO exchange with the Fe*CN metalloligand yielding complex **Fe*-2** in THF solution.

Scheme 2. Synthesis of **Fe-1**, **Fe*-1** as BF_4^- salts, and **Fe*-2**. The IR stretching frequencies of the diatomic ligands of the complexes in CH_2Cl_2 are shown below.

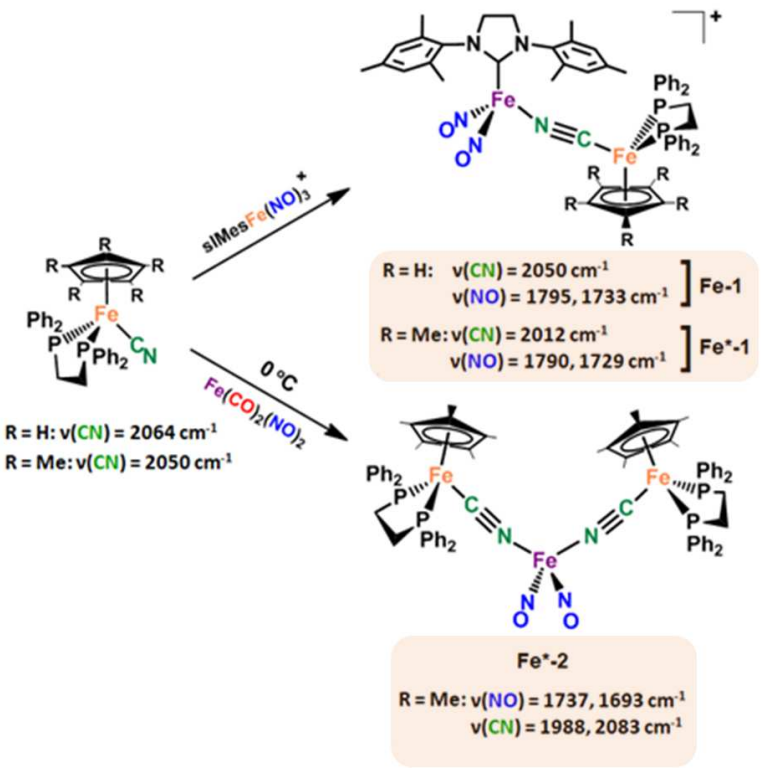

Positive-ion ESI mass spectrum of **Fe-1** and **Fe*-1** displayed characteristic signals at the molecular ion masses, *m/z* 967.28 and *m/z* 1037.33, respectively, with isotopic distribution patterns that closely matched the calculated bundle, for each diiron complex, Figures S18 and S19.† The X-band EPR spectra collected in perpendicular mode field polarization of frozen CH_2Cl_2 solutions of the paramagnetic **Fe-1** and **Fe*-1**, at 4 or 7 K, showed the presence of $S = 1/2$ species with coupling from the ^{14}N nuclei ($I_N = 1$) of CN, Figure 1. The g_{xyz} values and the coupling constants are provided in Figure 1. No coupling to NO was detected in the spectra from these complexes.

Freshly prepared $Fe(CO)_2(NO)_2$ at 0 °C in THF was used as precursor to generate the reduced, metallocyanide-bound $\{Fe(NO)_2\}^{10}$ adduct with (dppe)(η^5-C_5R_5)Fe(CN) as donor, Scheme 1. The product is thermally sensitive, requiring all manipulations to be carried out at -35°C. The presence of two cyano-iron donors, displaying C_2v local symmetry and symmetrical and asymmetrical ν(NO) and ν(CN) stretching vibrations within a triiron species, was confirmed by XRD and mass spectrometry. The ν(NO) values, at 1737 and 1693 cm^{-1}, are ca. 45 cm^{-1} lower than the corresponding metallocyanide-bound $\{Fe(NO)_2\}^9$ adduct, **Fe*-1**. The ν(CN) IR values of 2083 and 1988 cm^{-1} average to 2035 cm^{-1}, some 15 cm^{-1} lower overall than that of the reactant, ν(CN) = 2050 cm^{-1}. The positive-ion ESI mass spectrum of the product displayed a prominent signal at *m/z* 1346.47, which corresponded to [(dppe)(η^5-C_5Me_5)Fe-CN]$_2$-$Fe(NO)_2$, **Fe*-2**.

Molecular structures

The cyanide bridged adducts, **Fe-1** and **Fe*-1**, as BF_4^- salts, crystallized as purple and brown needles upon layering CH_2Cl_2 solutions with hexane at -30 ^oC. The **Fe*-2** co-crystallized with precursor **Fe*-CN** as thin brown plates via THF/pentane diffusion at -30 ^oC, under N_2. The molecular structures of **Fe*-CN**, **Fe-1**, **Fe*-1** and **Fe*-2** are shown in Figure 3 with selected metric parameters tabulated in Table 1. Full structural reports are deposited in the Cambridge Crystallographic Data Centre.

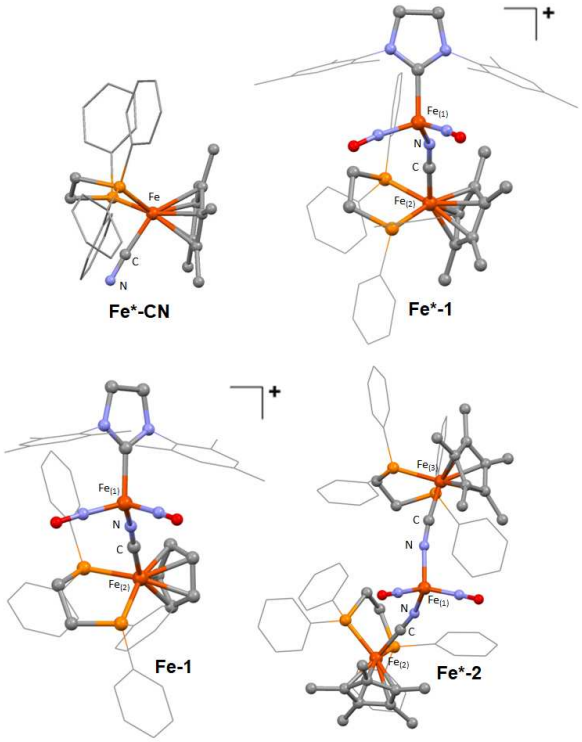

Figure 3. Ball and stick representations of the molecular structures of (dppe)(η^5-C_5Me_5)Fe(CN) (**Fe***), **Fe-1**, **Fe*-1** and **Fe*-2**. The phenyl and mesityl groups are represented as wire-forms; counter anions of **Fe-1** and **Fe*-1** are BF_4^-.

A pseudo tetrahedral geometry is observed at the $Fe_{(1)}$ center with C_{IMes}-$Fe_{(1)}$-N_{CN} (for **Fe-1** and **Fe***-1) or N_{CN}-$Fe_{(1)}$-N_{CN} (for **Fe*-2**) angle ranging from 110^o to 113^o and the N_{NO}-$Fe_{(1)}$-N_{NO} angle was ca. 114^o. The dinitrosyl iron units display the typical bent Fe-N-O, and the common 'attracto' orientation,[22] with individual $Fe_{(1)}$-N-O angles ranging from 156 to 171^o. The Fe^{II} center(s) in (dppe)(η^5-C_5R_5)Fe(CN) units displayed a typical piano stool coordination geometry with the dppe and cyanide as the tripodal base; there are no significant differences between the structures of the precursor and the μ-cyanoiron adducts.

Table 1. Selected metric parameters of **Fe-1**, **Fe*-1** and **Fe*-2**.

	Fe-1	**Fe*-1**	**Fe*-2**
∠$Fe_{(1)}$-N-C / ^{o}	165.2 (4)	152.6 (7)	156.8 (1) 168.5 (1) [c]
∠$Fe_{(2)}$-C-N / ^{o}	177.5 (4) *179.6 (4)* [a]	178.5 (7) *176.1 (3)* [b]	173.3 (1) 173.4 (1) [c]
∠$Fe_{(1)}$-N-O / ^{o}	166.4 (4) 170.7 (4)	164.9 (6) 165.3 (7)	156.9 (1) 171.0 (1)
$Fe_{(1)}$•••$Fe_{(2)}$ / □	4.941 (2)	4.820 (2)	4.889 (3) 4.880 (3) [c]
$Fe_{(1)}$-N / □	1.954 (4)	1.959 (8)	1.960 (1) 1.934 (9) [c]
C≡N / □	1.167 (5) *1.153 (7)* [a]	1.191 (1) *1.148 (4)* [b]	1.16 (2) 1.15 (2) [c]

[a,b] values in italics are for the starting materials dppe(η^5-C_5R_5)Fe(CN) (where R = H,[18] Me (**Fe*-CN**), respectively).

[c] for complex **Fe*-2**, two sets of values correlate to the metric assignments with two μ-cyano bridged species.

While the $Fe_{(2)}$-C-N angles in **Fe-1** and **Fe*-1** are almost linear, 177.5^o and 178.5^o, respectively, and similar to their precursors, the $Fe_{(1)}$-N-C angles show significant deviation from linearity. The extent of angular bend as observed for MC≡N-M', in M-C≡N-M' complexes, depend primarily on the electron density of the bridging N of the μ-cyano ligand and the electron polarizability of the second metal, M'. Extensive reports have noted the angular dependence of (por)Fe^{III}C≡N-Cu^{II} with regards to the geometry of the Cu^{II} center (distorted square pyramidal or distorted trigonal bipyramidal), with values as small as 147^o and as large as 173°.[5] In the present context, the angular bend for Fe^{II}C≡N-{$Fe(NO)_2$}^{9} was found to be 165.2^o for **Fe-1** and 152.6^o for **Fe*-1**. As the receiver unit, {$Fe(NO)_2$}^{9}, isolelectronic with Cu^{II} (d^9), maintains a pseudo tetrahedral geometry in both cases, the increase in electron density at the bridging N of the μ-cyanoiron ligand for **Fe*-1**, due to the η^5-C_5Me_5, should account for the marked angular deviation.

Two distinct Fe^{II}C≡N-{$Fe(NO)_2$}^{9}-N≡CFe^{II} angles, 156.8 and 168.5^o were observed for **Fe*-2**; the 12^o difference indicates non-equivalent orbital interaction with the two bridging cyanides, perhaps contributing to the distinct *v*(CN) stretching frequencies, *vide supra*. Such variation of bond angles were correlated with the increase in the (por)Fe^{III}CN-Cu^{II} bond length,[5] which remains almost invariant in the present case, ca. 1.95 □, Table 1. The greater Fe^{II}C≡N-{$Fe(NO)_2$}^{9} angular bends for **Fe*-1** and **Fe*-2** were reflected in the decrease of $Fe_{(1)}$•••$Fe_{(2)/(3)}$ distance by 0.121 □ and ca. 0.055 □, respectively, compared to **Fe-1**.

Electrochemistry

Cyclic voltammograms (CV) of **Fe-1** and **Fe*-1** as BF_4^- salts, and, for comparison, the starting materials, (dppe)(η^5-C_5R_5)Fe(CN), were recorded at 22 °C under Ar in CH_2Cl_2 containing 0.1 M

[^{t}Bu$_4$N][PF$_6$] as supporting electrolyte and referenced to $Fc^{+/0}$, using a glassy carbon working electrode. Figure 4 shows the scans at 200 mV/sec, with assignments listed therein. Scan rate overlays to determine reversibility or quasi-reversibility are given in Figures S11-S15.†

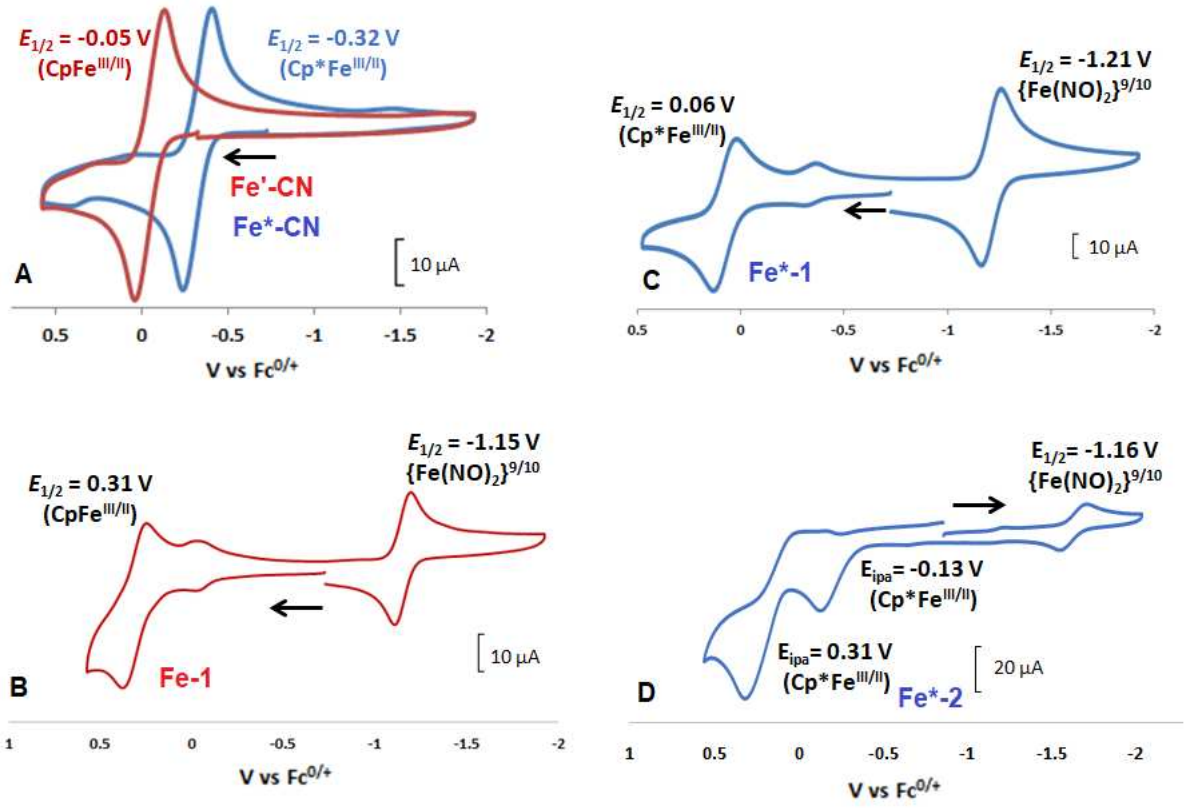

Figure 4. Cyclic voltammograms of A) overlay of (dppe)(η^5-C_5R_5)Fe(CN), where R = H (red), Me (blue); B) **Fe-1**; C) **Fe*-1** and D) **Fe*-2**.

While the starting materials, (dppe)(η^5-C_5R_5)Fe(CN) showed single reversible events at -0.05 and -0.32 V for the (η^5-C_5R_5)Fe$^{III/II}$ redox couples of R = H and CH_3, respectively, the complexes **Fe-1** and **Fe*-1**, overall showed two redox events, a reversible reduction, assigned to the {Fe(NO)$_2$}$^{9/10}$ couple and a quasi-reversible wave assigned to the (η^5-C_5R_5)Fe$^{III/II}$ event. The event at 0.31 V, assigned to the (η^5-C_5H_5)Fe$^{III/II}$ couple for the **Fe-1** complex, was shifted less positive by ca. 250 mV for **Fe*-1**, implying stabilization of the oxidized Fe due to the enriched electron donation by the η^5-C_5Me_5 unit. A similar shift was observed for the (η^5-C_5R_5)Fe$^{III/II}$ redox couple in the MN_2S_2•[Fe(η^5-C_5R_5)(CO)]$^+$ complexes, (M = [(NO)Fe]^{II}, [(NO)Co]^{II}, Ni^{II}].[23, 24] The effect of the enriched electron donor properties of the η^5-C_5Me_5 unit was conveyed via the bridging cyanide ligand, and felt, to a lesser extent, at the Fe(NO)$_2$ center. The reversible {Fe(NO)$_2$}$^{9/10}$ couple at -1.15 V for **Fe-1**, was shifted by 60 mV more negative for **Fe*-1** ($E_{1/2}$ = -1.21 V), indicating greater stabilization of the {Fe(NO)$_2$}^{9} state of the latter. Minor redox features were

observed at ~ -0.05 and ~ -0.32 V for **Fe-1** and **Fe*-1** complexes, respectively, and assigned to the (η^5-C_5R_5)$Fe^{II/III}$ redox couple of (dppe)(η^5-C_5H_5)Fe(CN)and (dppe)(η^5-C_5Me_5)Fe(CN), respectively, as impurities. Repeated scans, however, did not show an increase in the current intensity of these redox features, indicating no further decomposition of **Fe-1** and **Fe*-1** complexes at the electrode surface, Figure S16-17. †

The cyclic voltammogram of **Fe*-2** was recorded at ~ -5 ^oC, under argon, using a glassy carbon working electrode, with 0.1 M [$^tBu_4N$][PF_6] supporting electrolyte THF solution, Figure 4(D). A reversible redox event, assigned to the $\{Fe(NO)_2\}^{9/10}$ couple, was observed at -1.16 V. The value indicates greater ease of reduction, compared to the $\{Fe(NO)_2\}^{9/10}$ redox couple of **Fe*-1** (-1.21 V), by around 60 mV. Two irreversible cathodic events were observed at -0.13 and 0.31 V, assigned to the sequential oxidation of (η^5-C_5R_5)$Fe^{III/II}$ units. The scan rate dependence studies of **Fe*-2** for the $\{Fe(NO)_2\}^{9/10}$ couple are shown in Figure S15.†

Reactivity Studies

In an attempt to test the lability of Fe^{II}-CN-$\{Fe(NO)_2\}^{9/10}$ bond, the complexes **Fe-1**, **Fe*-1** and **Fe*-2** were exposed to nucleophiles, of various electronic and steric features, Scheme 2. Treatment of **Fe-1** and **Fe*-1** with Na^+SPh^-, showed an immediate displacement of (dppe)(η^5-C_5R_5)Fe(CN), with concomitant formation of sIMesFe$(NO)_2$(SPh). The IR spectral monitor indicated a shift in the ν(NO) vibrational bands from 1795, 1733 cm^{-1} (**Fe-1**) or 1790, 1729 cm^{-1} (**Fe-1***) to 1763, 1715 cm^{-1}, consistent with the known values of sIMesFe$(NO)_2$(SPh).[20], Figure S3-4.†

With 7 equivalents of added PMe_3, ligand substitution on **Fe-1** and **Fe*-1** occurred over the course of ca. 3 h, in both cases effecting a complete shift in ν(NO) values to 1705, 1660 cm^{-1} (THF), along with ν(CN) stretches corresponding to the freed (dppe)(η^5-C_5R_5)Fe(CN). The ν(NO) bands in both cases indicated formation of $L_2Fe(NO)_2$, (L = PMe_3). This result was similar to the reaction of sIMesFe$(NO)_2$(SPh) with PMe_3 that also showed ν(NO) vibrational bands at 1705, 1659 cm^{-1}. The product was isolated and characterized using ^{31}P NMR spectroscopy and the X-ray diffraction studies confirmed the compound was $(Me_3P)_2Fe(NO)_2$. The $(Me_3P)_2Fe(NO)_2$ complex derived in this fashion was diamagnetic, indicating a reduced $\{Fe(NO)_2\}^{10}$ species, formed by the simultaneous oxidation of PhS^- to diphenyldisulfide. Thus, the aforementioned reactions of **Fe-1** and **Fe*-1** with PMe_3, led to a double substitution of the sIMes and dppe(η^5-C_5R_5)Fe(CN) with the concomitant reduction of the DNIU from $\{Fe(NO)_2\}^9$ to $\{Fe(NO)_2\}^{10}$. Reactions of **Fe-1** and **Fe*-1**, with PPh_3 (> 10 equiv.) over a period of 12 h, however, did not show a displacement of the (dppe)(η^5-C_5R_5)Fe(CN). Neither was there reaction with CO, bubbled at 1 atm.

The identity of $L_2Fe(NO)_2$ as $(Me_3P)_2Fe(NO)_2$ from such reactions was further established upon treating **Fe*-2**, having a reduced $\{Fe(NO)_2\}^{10}$ DNIU, with PMe_3 at 0 °C. The ν(NO) spectral monitor showed a shift in the ν(NO) vibrational frequencies from 1737, 1693 cm^{-1} to 1705, 1660 cm^{-1} (THF); the displaced (dppe)(η^5-C_5Me_5)Fe(CN) was identified by its characteristic ν(CN) stretching frequencies.

Scheme 3. Ligand exchange studies of **Fe-1**, **Fe*-1** and **Fe*-2** with various nucleophiles.

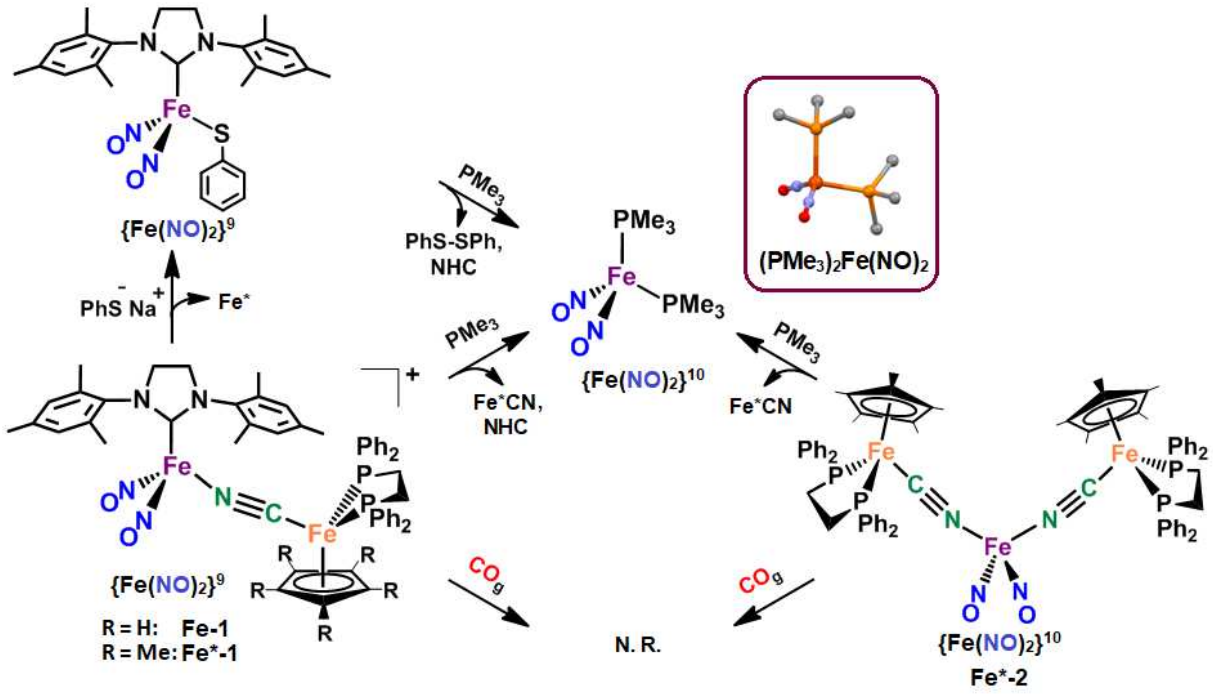

Conclusion

Three bi-/trimetallic molecular complexes containing Fe^{II}-CN-$\{Fe(NO)_2\}^{9/10}$ unit were synthesized and structurally characterized, establishing the role of cyanide as a bridging ambidentate ligand. The question of whether the dinitrosyliron units (DNIU), $\{Fe(NO)_2\}^9$ and $\{Fe(NO)_2\}^{10}$, as delocalized electronic analogs of the isoelectronic Cu^{II} and Cu^{I}, d^9 and d^{10}, respectively, was only partially answered; the binding occurs, however no linkage isomerism or flipping was seen.[5,9] Our studies were inspired as mimics of cyanide's ambidentate ligating attributes with reference to biological cyanide-inhibited cytochrome-C oxidase as well as in Hyd-F of [FeFe]-H_2ases. We found that the L-type neutral μ-cyanoiron metalloligands indeed bound to the DNIU in both $\{Fe(NO)_2\}^9$ and $\{Fe(NO)_2\}^{10}$ redox states, however the Fe^{II}-CN orientation of the starting cyanoiron(II) complex precursor was maintained in both. As our mechanistic understanding of cyanide flipping in bioorganometallic mimetics increases,[13,14] we ascribe the difference in propensities of the redox levels of copper vs DNIU towards C vs. N bound cyanide to the lack of an easy path towards isomerization in the delocalized DNIU.[13,14] The lability of the

Fe^{II}-CN-$\{Fe(NO)_2\}^{9/10}$ bond was examined with different nucleophiles that showed loss of the μ-cyanoiron metalloligand always with cleavage at the N-Fe. Reduction of $\{Fe(NO)_2\}^9$ to $\{Fe(NO)_2\}^{10}$ was observed concommitant with exchange of L-type PMe_3, but no redox changes were seen with X-type Na^+SPh^-. No exchange was seen under a blanket of CO_g and likewise the bulky PPh_3 failed. These interesting ligand substitution reactions, and phosphine-induced reduction, are the subject of an ongoing kinetic and mechanistic study.

EXPERIMENTAL SECTION

Methods and Materials.

Solvents, dichloromethane (CH_2Cl_2), methanol (MeOH) hexane, pentane and diethylether, were purified and degassed on the MBraun Manual Solvent Purification System with Alcoa F200 activated alumina desiccant. Tetrahydrofuran (THF) was freshly distilled after reflux in the presence of sodium and benzophenone. Standard Schlenk conditions under N_2 and Ar atmospheres were used to carry out all reactions. All reagents were used as received from standard vendors unless otherwise stated. The complexes, (dppe)(η^5-C_5H_5)Fe(CN) (**Fe'-CN)**,[18] [(sIMes)Fe$(NO)_3$][BF_4],[20, 25] $Fe(CO)_2(NO)_2$,[19] (sIMes)Fe$(NO)_2$(SPh)[20, 25] and (dppe)(η^5-C_5Me_5)FeCl[26] were prepared according to published procedures; sIMes = the N-heterocyclic carbene, NHC, was derived from 1,3-bis(2,4,6-trimethylphenyl)imidazolinium chloride. HPLC-grade acetonitrile, [n-Bu_4N][PF_6], Na^+SPh^- and $Fc^+PF_6^-$ were reagent grade and purchased from Sigma-Aldrich.

Physical Measurements. Solution infrared spectra were recorded using the Bruker Tensor 37 Fourier transform IR (FTIR) spectrometer and a CaF_2 cell of 0.2 mm path length. All mass spectrometry (ESI-MS) was provided and performed by the laboratory for Biological Mass Spectrometry at Texas A&M University. The Inova 500 MHz superconducting NMR instrument was used to acquire ^{1}H NMR, ^{13}C NMR, and ^{31}P NMR spectra. Cyclic voltammograms (CV's) were recorded on the CHI600E electrochemical analyzer (HCH instruments, Inc.) using a three-electrode cell: a) working electrode a 0.071 cm^2 glassy carbon disc; counter electrode, a platinum wire; reference electrode, a CH_3CN solution of $Ag/AgNO_3$ in a Vycor-tipped glass tube. Throughout the CV experiments, diamond paste (3 μm) was used to polish the glassy carbon electrode as needed. Solutions used in CV scans were purged with Ar for 5 min and a blanket of Ar was kept over the solution during the experiments. Solutions (2.0 mM) of **Fe-1**, **Fe*-1**, and **Fe*-CN** (DCM) contained 0.1 M [n-Bu_4N][PF_6] as the electrolyte. A 2.0 mM THF solution of **Fe*-2 ,** containing 0.1 M [n-Bu_4N][PF_6] as the electrolyte was kept at ~ -5 °C. The Fc/Fc^+ couple at 0.00 V was used as an internal reference for all reported potentials.

X-ray Diffraction Analyses. The crystal data for **Fe-1**, **Fe*-1**, and **Fe*-2** were determined with the BRUKER Venture X-ray (kappa geometry) diffractometer with Cu-Iμs X-ray tube (K_α = 1.5418Å) at 100 K. The **Fe*-CN** crystal structure was measured with the BRUKER APEX 21 X-ray (three-circle) diffractometer with Mo sealed X-ray tube (K_α = 0.70173Å) at 110 K. Weighted least squares refinement on F^0 was used for refining the structures. At idealized positions, hydrogen atoms were placed and fixed isotropic displacement parameters were used to refine them. Anisotropic displacement parameters were employed for all non-hydrogen atoms.The following programs were used: data collection, APEX3;[27] data reduction, SAINT;[28] absorption correction, SADABS;[29] cell refinement and structure solutions, SHELXS/XT;[29] The final data presentation and structure plots were generated in Olex2.[30] Crystallographic data for the complexes **Fe-1**, **Fe*-1**, **Fe*-2**, **Fe*-CN**, and **$(PMe_3)_2Fe(NO)_2$** are deposited in the Cambridge Crystallographic Data Centre; their numbers are: CCDC 1840853 (**Fe-1**), CCDC 1840809 (**Fe*-1**), CCDC 1840824 (**Fe*-2**), CCDC 1840810 (**Fe*-CN**), and CCDC 1840854 (**$(PMe_3)_2Fe(NO)_2$**). Crystal data and structure refinement parameters are summarized in Tables T21-25.

Syntheses

[(dppe)(η^5-C_5Me_5)Fe(CN)], (Fe*-CN). A 0.50 g (0.81 mmol) portion of (dppe)(η^5-C_5Me_5)Fe(Cl) and 0.27 mg (4.1 mmol) of KCN were placed in a 100 mL Schlenk flask, and the contents were dissolved in MeOH; the resulting orange solution was stirred overnight. The solvent was removed in vacuo, and the residue was extracted with CH_2Cl_2. The CH_2Cl_2 solution was filtered through celite to remove any unreacted starting material. X-ray quality crystals for complex **Fe*-CN** were obtained by layering a CH_2Cl_2 solution of the product with pentane. IR (CH_2Cl_2, cm^{-1}): *ν*(CN) 2050; ESI-MS^+: *m/z* 638.18 (for [M] + Na^+).

[((dppe)(η^5-C_5H_5)Fe-CN-Fe$(NO)_2$(IMes)][BF_4], (Fe-1). As described above, 0.11 g (0.20 mmol) of (dppe)(η^5-C_5H_5)Fe(CN) and 0.12 g (0.22 mmol) of [(sIMes)Fe$(NO)_3$][BF_4] were added in a 100 mL Schlenk flask, and the contents were dissolved in CH_2Cl_2; the resulting dark purple solution was stirred for 10 min. Dichloromethane was removed in vacuo and the resulting solids were washed once with ether/hexane (1:1, v/v) and twice with hexane. The purple solid was redissolved in CH_2Cl_2 and filtered through celite to remove any possible solid insoluble impurities. X-ray quality crystals for complex **Fe-1** were obtained by layering a CH_2Cl_2 solution of the product with pentane at -30 °C. IR (CH_2Cl_2, cm^{-1}): *ν*(CN) 2050; *ν*(NO) 1795, 1733. ESI-MS^+: *m/z* 967.28.

[(dppe)(η^5-C_5Me_5)Fe-CN-Fe$(NO)_2$(IMes)][BF_4], (Fe*-1). The reaction conditions, reaction work up, and recrystallization methods used for **Fe*-1** were the same as **Fe-1** except 0.12 g (0.20 mmol) of (dppe)(η^5-C_5Me_5)Fe(CN) (**Fe*-CN**) and 0.12 mg (0.22 mmol) of [(sIMes)Fe$(NO)_3$][BF_4] were

dissolved in CH_2Cl_2 giving an emerald green solution. IR (CH_2Cl_2, cm^{-1}): *v*(CN) 2012; *v*(NO) 1790, 1729. ESI-MS^+: *m/z* 1037.33.

[(dppe)(η^5-C_5Me_5)Fe-CN]$_2$-Fe(NO)$_2$, (Fe*-2). Approximately 0.2 mmol of $Fe(CO)_2(NO)_2$ in THF was prepared in a 50 mL Schlenk flask according to previously reported procedures and was condensed into a 50 mL Schlenk flask placed into a Dewar flask filled with liquid N_2 containing 0.61 g (0.11 mmol) of (dppe)(η^5-C_5Me_5)Fe(CN) through a vacuum adapter. After the condensation of $Fe(CO)_2(NO)_2$, removal of Schlenk flask from Dewar, and replacement of the vacuum adapter, the reaction flask was placed in a -10 °C acetone/ice bath to thaw the contents and then stirred for 30-45 min. The reaction was monitored by IR spectroscopy and upon no further changes, the solvent was removed in vacuo, maintaining a temperature of -5 °C to also remove the volatile $Fe(CO)_2(NO)_2$. The dark brown solid was redissolved in THF and filtered quickly through celite to remove any insoluble impurities while maintaining the temperature at -5 °C. IR (CH_2Cl_2, cm^{-1}): *v*(CN) 2083, 1988; *v*(NO) 1737, 1693: ESI-MS^+: *m/z* 1346.47.

(Me$_3$P)$_2$Fe(NO)$_2$. In a 50 mL Schlenk flask 0.050 g (0.10 mmol) of (sIMes)$Fe(NO)_2$(SPh) was dissolved in 20 mL of THF and reacted with excess PMe_3 (0.20 mL, 2.0 mmol) by stirring at room temperature. Reaction completion and formation of $(Me_3P)_2Fe(NO)_2$ was monitored by IR spectroscopy. The solvent and excess PMe_3 were removed *in vacuo*. The orange-red solid was dissolved in THF then filtered through celite. X-ray quality crystals for complex $(Me_3P)_2Fe(NO)_2$ were obtained by layering a THF solution of the product with pentane. IR (THF, cm^{-1}): *v*(NO) 1705, 1659: Elemental Anal. Calculated for $FeC_6CH_{18}N_2O_2P_2$ (found): C, 29.70 (28.94); H, 7.48 (7.05); N, 9.90 (9.57). $^{31}P\{^1H\}$ NMR (THF): δ 14.3 (s, 2P).

Dedication: With congratulations to Distinguished Professor Kim Dunbar at this milestone and with appreciation for her collegiality and wonderful contributions as a committee member to scores of graduate students, including those contributors to this manuscript.

Acknowledgements

We sincerely thank the National Science Foundation for financial support (CHE-1266097 and CHE-1665258), and the Robert A. Welch Foundation (A-0924). Appreciation is expressed to Dr. Xianggao Meng for assisting in XRD analysis.

Notes and references

‡Equally contributing authors

Corresponding author:
*marcetta@chem.tamu.edu

†Electronic Supplementary Information (ESI) available: See DOI: 10.1039/x0xx00000x

References

1. K. R. Dunbar and R. A. Heintz, *Progress in Inorg. Chem.*, 2007, **45**, 283.
2. K. E. Funck, M. G. Hilfiger, C. P. Berlinguette, M. Shatruk, W. Wernsdorfer and K. R. Dunbar, *Inorg. Chem*., 2009, **48**, 3438.
3. D. -Q. Wu, D. Shao, X. -Q. Wei, F. -X. Shen, L. Shi, D. Kempe, Y. -Z. Zhang, K. R. Dunbar and X. -Y. Wang *J. Am. Chem. Soc.*, 2017, **139**, 11714.
4. S. C. Lee, M. J. Scott, K. Kauffmann, E. Münck and R. H. Holm, *J. Am. Chem. Soc*., 1994, **116**, 401.
5. M. J. Scott and R. H. Holm, *J. Am. Chem. Soc*., 1994, **116**, 11357.
6. M. T. Gardner, G. Deinum, Y. Kim, G. T. Babcock, M. J. Scott and R. H. Holm. *Inorg. Chem*., 1996, **35**, 6878.
7. M. J. Scott, S. C. Lee and R. H. Holm, *Inorg. Chem*., 1994, **33**, 4651.
8. S. B. Lim and R. H. Holm, *Inorg. Chem*., 1998, **37**, 4898.
9. D. M. Corsi, N. N. Murthy, V. G. Young, Jr. and K. D. Karlin, *Inorg. Chem*., 1999**, 38**, 848.
10. A. Geiss and H. Vahrenkamp, *Inorg. Chem*., 2000**, 39**, 4029.
11. A. Geiss, M. J. Kolm, C. Janiak and H. Vahrenkamp, *Inorg. Chem*., 2000**, 39**, 4037.
12. G. Berggren, A. Adamska, C. Lambertz, T. R. Simmons, J. Esselborn, M. Atta, S. Gambarelli, J. -M. Mouesca, E. Reijerse, W. Lubitz, T. Happe, V. Artero and M. Fontecave, *Nature*, 2013, **499**, 66.
13. A. M. Lunsford, C. C. Beto, S. Ding, Ö. F. Erdem, N. Wang, N. Bhuvanesh, M. B. Hall and M. Y. Darensbourg, *Chem*. *Sci*., 2016, **7**, 3710.
14. D. Sil, Z. Martinez, S. Ding, N. Bhuvanesh, D. J.Darensbourg, M.B. Hall, M.Y. Darensbourg **"**Model Studies of Cyanide Docking and Linkage Isomerism in Artificial Maturation of [FeFe]-Hydrogenase", manuscript submitted to the J. Am. Chem. Soc.
15. J. H. Enemark and R. D. Feltham, *Coord*. *Chem*. *Rev*., 1974, **13**, 339–406.
16. C. –H. Hsieh, S. Ding, O. F. Erdem, D. J. Crouthers, T. Liu, C. C. L. McCrory, W. Lubitz, C. V. Popescu, J. H. Reibenspies, M. B. Hall and M. Y. Darensbourg, *Nat*. *Commun*., 2014, **5**, 3684
17. P. Ghosh, S. Ding, R. B. Chupik, M. Quiroz, C. -H. Hsieh, N. Bhuvanesh, M. B. Hall and M. Y. Darensbourg, *Chem. Sci.*, 2017, **8**, 8291.
18. D. J. Darensbourg, M. J. Adams, J. C. Yarbrough and Andrea L. Phelps, *Eur. J. Inorg. Chem*., 2003, **3639**, 3648.
19. D. W. McBride, S. L. Stafford and F. G. A. Stone, *Inorg. Chem.*, 1962, **1**, 386.
20. C. H. Hsieh and M. Y. Darensbourg, *J. Am. Chem. Soc*., 2010,**132**, 14118.
21. C. H. Hsieh, R. B. Chupik, T. Pinder and M. Y. Darensbourg, *Polyhedron*, 2013**, 58**, 151.
22. G. B. Richter-Addo and P. Legzdins, Metal Nitrosyls, Ch. 5 Oxford University Press (1992) **ISBN-10:** 0195067932
23. S. Ding, P. Ghosh, A. M. Lunsford, N. Wang, N. Bhuvanesh, M. B. Hall and M. Y. Darensbourg, *J. Am. Chem. Soc.*, 2016, **138**, 12920.

24. P. Ghosh, M. Quiroz, N. Wang, N. Bhuvanesh and M. Y. Darensbourg, *Dalton Trans*., 2017, **46**, 5617.
25. R. Pulukkody, S. J. Kyran, M. J. Drummond, C.–H. Hsieh, D. J. Darensbourg and M. Y. Darensbourg, *Chem. Sci.*, 2014, **5**, 3795.
26. D. Patel, A. Wooles, A. D. Cornish, L. Steven, E. S. Davies, D. J. Evans, J. McMaster, W. Lewis, A. J. Blake and S. T. Liddle, *Dalton Trans.*, 2015, **44**, 14159.
27. *APEX2*, Bruker AXS Inc., Madison, WI, 2007.
28. *SAINT*, Bruker AXS Inc., Madison, WI, 2007.
29. G. Sheldrick, *Acta*. *Cryst*., 2008, *A64*, 112. (2)
30. O. V. Dolomanov, L. J. Bourhis, R. J. Gildea, J. A. K. Howard and H. Puschmann, *J. Appl. Cryst.*, 2009*,* **42**, 339–341.

101x56mm (144 x 144 DPI)